Supplementary Information

Metal-(organic cocrystal) Framework with Photothermal Effect Boosting Photocatalytic Degradation of Pollutants

Mengran Liu,[+] Kexin Liu,[+] Zhuang Yan, Chenfei Yang, Shouzhen Li, Yi Su, Kuo Yuan, Xiaotao Zhang,* Wenping Hu*

Table of Contents

1. General Information

Reagents.

5,5'-(1,3,6,8-tetraoxo-1,3,6,8-tetrahydrobenzo[lmn][3,8]phenanthroline-2,7-diyl)dibenzene-1,3-dicarboxylic acid (H_4BINDI, 98%) was procured from Shanghai Pedder Medical Technology Co., LTD. Acridine ($C_{13}H_9N$, 98%), calcium nitrate tetrahydrate ($Ca(NO_3)_2 \cdot 4H_2O$, 99.98%), and *N,N*-dimethylformamide (DMF, HPLC) were obtained from Shanghai Aladdin Biochemical Technology Co., LTD. All chemicals were used without further purification.

Synthesis of Ca-NDI MOF

The synthesis of Ca-NDI MOF was carried out following previously reported procedures. H_4BINDI (21 mg) and $Ca(NO_3)_2$ (28 mg) were added to a 15 mL pressure-resistant vial, followed by the addition of 4 mL of DMF and 0.2 mL of 3 M hydrochloric acid (HCl). After sonication for 0.5 hours, the mixture was heated at 100 °C for 24 hours. The yellow block crystals were obtained after slowly cooling to room temperature.

Synthesis of Ac@[Ca-NDI] MOCF

H_4BINDI (21 mg), $Ca(NO_3)_2$ (28 mg), and acridine (62.5 mg) were added to a 15 mL pressure-resistant vial, followed by the addition of 4 mL of DMF and 0.6 mL of 3 M hydrochloric acid (HCl). After sonication for 0.5 hours, the mixture was reacted at 100 °C for 24 hours. The dark green block crystals were obtained after slowly cooling to room temperature.

During the synthesis of Ac@[Ca-NDI] MOCF, the amount of acridine (Ac) was optimized to 62.5 mg. Although the theoretical stoichiometric ratio of H_4BINDI to Ac is 2:1, we found that using an excess of Ac (approximately 1:10) resulted in more ordered and purer MOCF crystals. When the amount of Ac was not in excess, the crystals often contained Ca-NDI MOF that had not effectively combined with Ac, which negatively impacted the purity of Ac@[Ca-NDI] MOCF. The excess Ac dissolved in the DMF solvent, ensuring that the final MOCF material maintained high purity.

Photothermal Experiments

A sample of 90 mg of MOCF powder was placed in a quartz cell and irradiated with an 808 nm laser at a power density of 0.6 W/cm^2. The heating and cooling curves were recorded to calculate the photothermal conversion efficiency. An infrared thermal imaging camera was used to monitor the temperature changes and capture photothermal images of the powder. The laser power density was adjusted to 0.2 W/cm^2, 0.4 W/cm^2, 0.6 W/cm^2 and 0.8 W/cm^2 to test the power density-dependent curves. The photothermal conversion efficiency was calculated using the following method:

$$\sum_i m_i C_{p,i} \frac{dT}{dT} = Q_S - Q_{loss}$$

where m_i is the total mass of the system during the photothermal test, $C_{p,i}$ is the specific heat capacity of the Ac@[Ca-NDI] MOCF, Q_S is the photothermal energy input to the Ac@[Ca-NDI] MOCF under 808 nm laser irradiation, and Q_{loss} is the heat energy lost to the surroundings. When the temperature of the Ac@[Ca-NDI] MOCF reaches its maximum value, the system reaches equilibrium:

$$Q_S = Q_{loss} = hS\Delta T_{max}$$

where h is the heat transfer coefficient, S is the surface area of the system, and ΔT_{max} is the maximum temperature change of the system. Therefore, the photothermal conversion efficiency of the Ac@[Ca-NDI] MOCF is calculated as:

$$\eta = \frac{hS\Delta T_{max}}{I\left(1-10^{-A_{808}}\right)}$$

where η is the photothermal conversion efficiency, I is the laser power, and A_{808} is the absorbance of the Ac@[Ca-NDI] MOCF at 808 nm. To obtain the value of hS, a dimensionless driving temperature θ is introduced:

$$\theta = \frac{T - T_{surr}}{T_{max} - T_{surr}}$$

where T is the real-time temperature of the Ac@[Ca-NDI] MOCF during illumination, T_{surr} is the initial temperature, and T_{max} is the maximum temperature reached by the system. The time constant τ_s

$$\tau_s = \frac{\sum_i m_i C_{p,i}}{hS}$$

From this, the equation becomes:

$$\frac{d\theta}{dt} = \frac{1}{\tau_s} \frac{Q_S}{hS\Delta T_{max}} - \frac{\theta}{\tau_s}$$

When the laser is turned off, $Q_S = 0$, $\frac{d\theta}{dt} = -\frac{\theta}{\tau_s}$, therefore, $t = -\tau_s \ln \theta$

By calculating hS from the slope of the cooling time (t) against $\ln \theta$, the final photothermal conversion efficiency of the Ac@[Ca-NDI] MOCF is found to be 70.65%.

Separately, 30 mg of the powder was dispersed in an aqueous solution at a concentration of 1 mg/mL. This dispersion was irradiated with a 300 W Xe lamp covering a wavelength range of 300 nm < λ < 1200 nm, with the light source positioned approximately 10 cm above the liquid surface. An infrared thermal imaging camera was used to monitor the temperature changes.

Photocatalytic Experiments

Under irradiation by a 300 W Xe lamp with a wavelength range of 300 nm < λ < 1200 nm, the photocatalytic performance of the MOCF was evaluated by degrading phenol pollutants (30 mg/L). Prior to photocatalytic degradation, the catalyst-phenol solution was stirred in the dark for 30 minutes to reach adsorption-desorption equilibrium. During the degradation process, samples were taken every 20 minutes, and the phenol concentration was determined using the 4-aminoantipyrine spectrophotometric method.

The main detection principle was as follows: At pH = 10 ± 0.2, phenolic compounds reacted with 4-aminoantipyrine in the presence of potassium ferricyanide to form a red antipyrine dye. After color development, the absorbance at 510 nm was measured within 30 minutes using a UV-Vis spectrophotometer.

The specific experimental steps were as follows: 2% 4-aminoantipyrine Solution: Weighed 2.0 g of 4-aminoantipyrine powder, dissolved it in a beaker, and diluted to 100 mL with water in a volumetric flask. Stored the solution in the dark.

pH = 10 Buffer Solution: Dissolved 5.4 g of ammonium chloride in 20.0 mL of water, added 35.0 mL of concentrated ammonia solution, and diluted to 100 mL with water.

8% Potassium Ferricyanide Solution: Weighed 8.0 g of potassium ferricyanide, dissolved it in a beaker, and diluted to 100 mL with water in a volumetric flask.

To perform the analysis, took 2 mL of the phenol solution into a centrifuge tube, filtered it, and diluted to 10 mL. Sequentially added 0.1 mL of buffer solution, 0.2 mL of 4-aminoantipyrine solution, and 0.2 mL of potassium ferricyanide solution. Mixed thoroughly and let stand for 10 minutes. Measured the

absorbance at 510 nm using a spectrophotometer.

Computational Details.

The primitive cells of Ac@[Ca-NDI] MOCF and Ca-NDI MOF models were selected for electronic structure investigations. These models underwent geometric optimization using the PBE functional within the framework of Density Functional Theory (DFT), incorporating the DFT-D3 dispersion correction for improved accuracy in modeling van der Waals interactions. Plane-augmented-wave (PAW) pseudopotentials were employed with an energy cutoff of 350 eV for all calculations. The optimization was carried out using the Vienna Ab initio Simulation Package (VASP), with ionic and electronic convergence criteria set to 0.05 eV $Å^{-1}$ and 10^{-6} eV, respectively. A k-point grid of 1×1×1 was used for the geometric optimization of all models. Following this, electronic band structures and density of states (DOS) plots were calculated using the PBE functional. For these electronic structure calculations, a denser k-point grid, generated by the Vaspkit tool, was employed to ensure high accuracy in the results.

Material characterization

The crystal structure was characterized on an X-ray diffractometer (XtaLAB Fr-X) using Cu Kα radiation (45 kV, 66 mA). Powder X-ray Diffraction (PXRD) patterns were obtained by a Rigaku Smart Lab 9 KW with Cu Kα radiation (λ = 1.542 Å) operating at 45 kV and 200 mA. The steady photoluminescence (PL) spectra were recorded with an Edinburgh instrument (FLS1000). Ultraviolet-visible (UV-vis) analysis was performed on a Shimadzu UV-3600 Plus spectrophotometer. Fourier transform infrared spectra (FTIR) were obtained on a Bruker Vertex 70 FTIR spectrometer. Ultraviolet photoelectron spectroscopy (UPS) measurements were carried out on a Thermo Scientific Escalab 250Xi spectrometer. He I was used as the excitation source with an energy of 21.22 eV. Gold specimens (Fermi edge at 0.0 eV) were used to calibrate the instrument. Thermogravimetric analysis (TGA) was performed by MettlerToledo TGA 2 thermal analysis system.

2. Supplementary Figures

Figure S1. Optical image of Ca-NDI MOF.

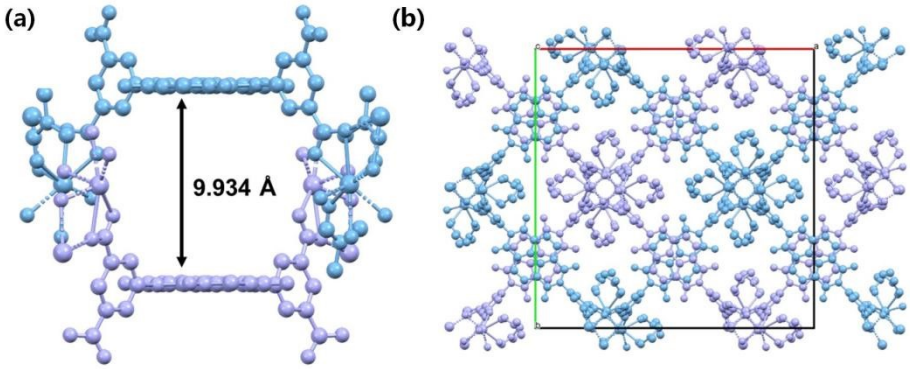

Figure S2. Crystal structure of Ca-NDI MOF (a) along the *a*-axis and (b) along the *c*-axis.

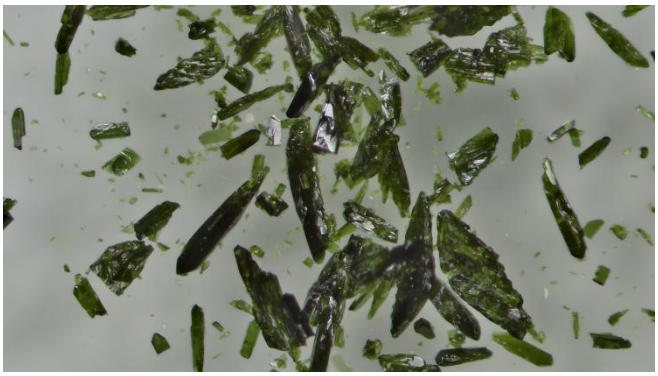

Figure S3. Optical image of Ac@[Ca-NDI] MOCF.

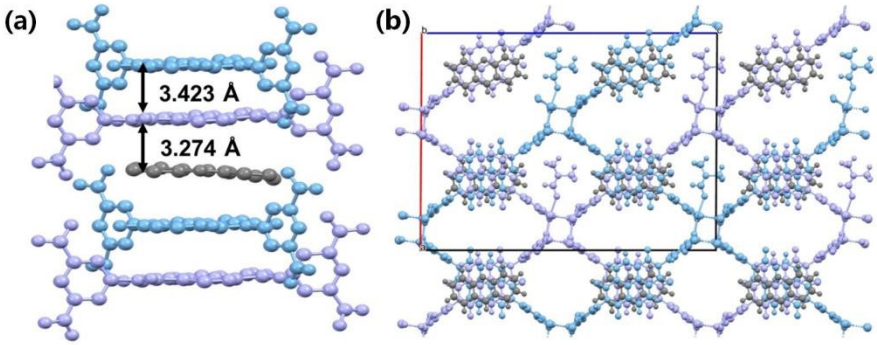

Figure S4. Crystal structure of Ac@[Ca-NDI] MOCF along the (a) *a*-axis and (b) *b*-axis.

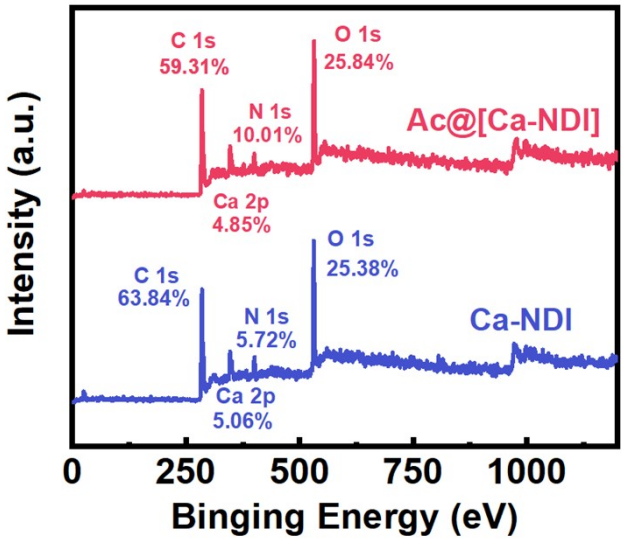

Figure S5. X-ray photoelectron spectroscopy of Ac@[Ca-NDI] MOCF and Ca-NDI MOF.

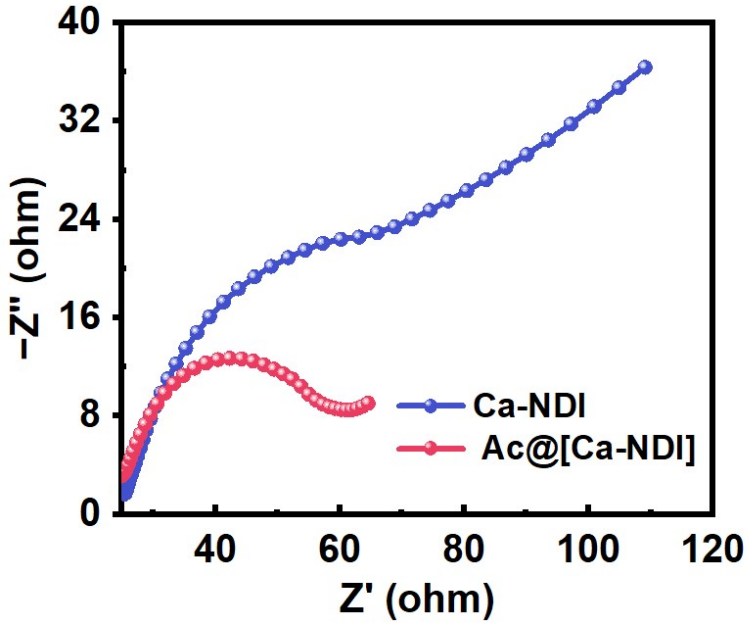

Figure S6. Electrochemical Impedance Spectroscopy (EIS) spectra of Ac@[Ca-NDI] MOCF and Ca-NDI MOF.

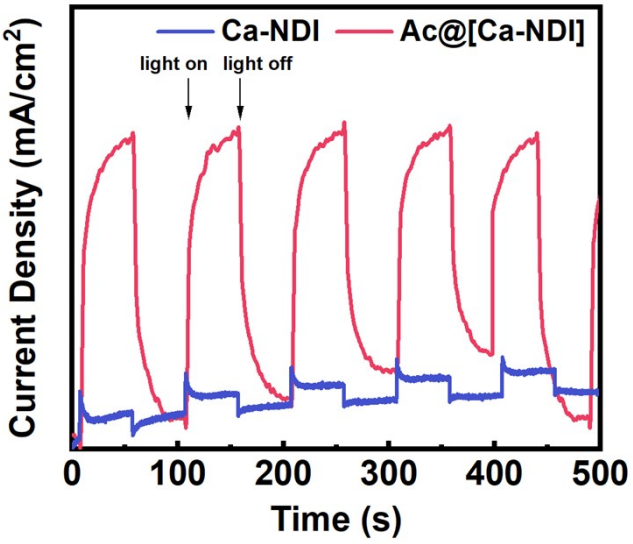

Figure S7 Photocurrent response results of Ac@[Ca-NDI] MOCF and Ca-NDI MOF.

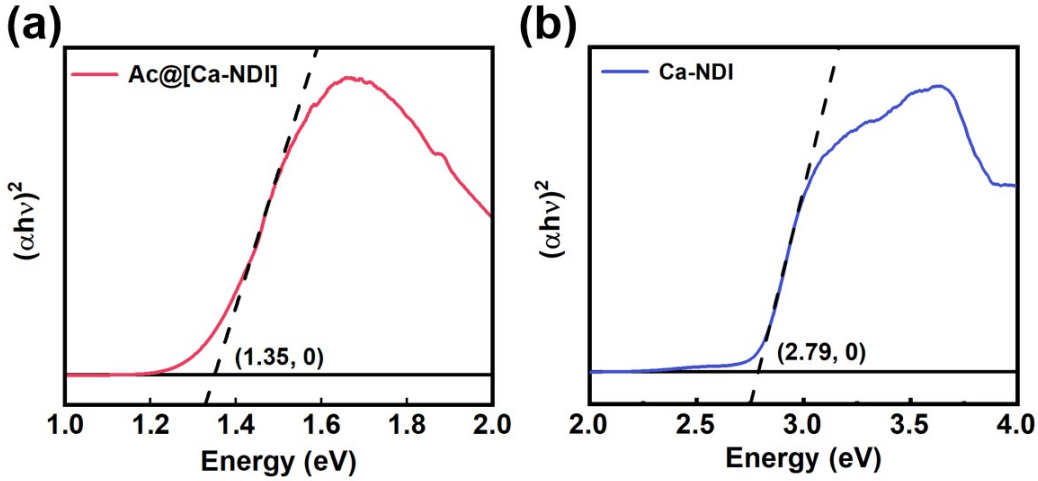

Figure S8. Band gap (*Eg*) diagrams of Ac@[Ca-NDI] MOCF and Ca-NDI MOF.

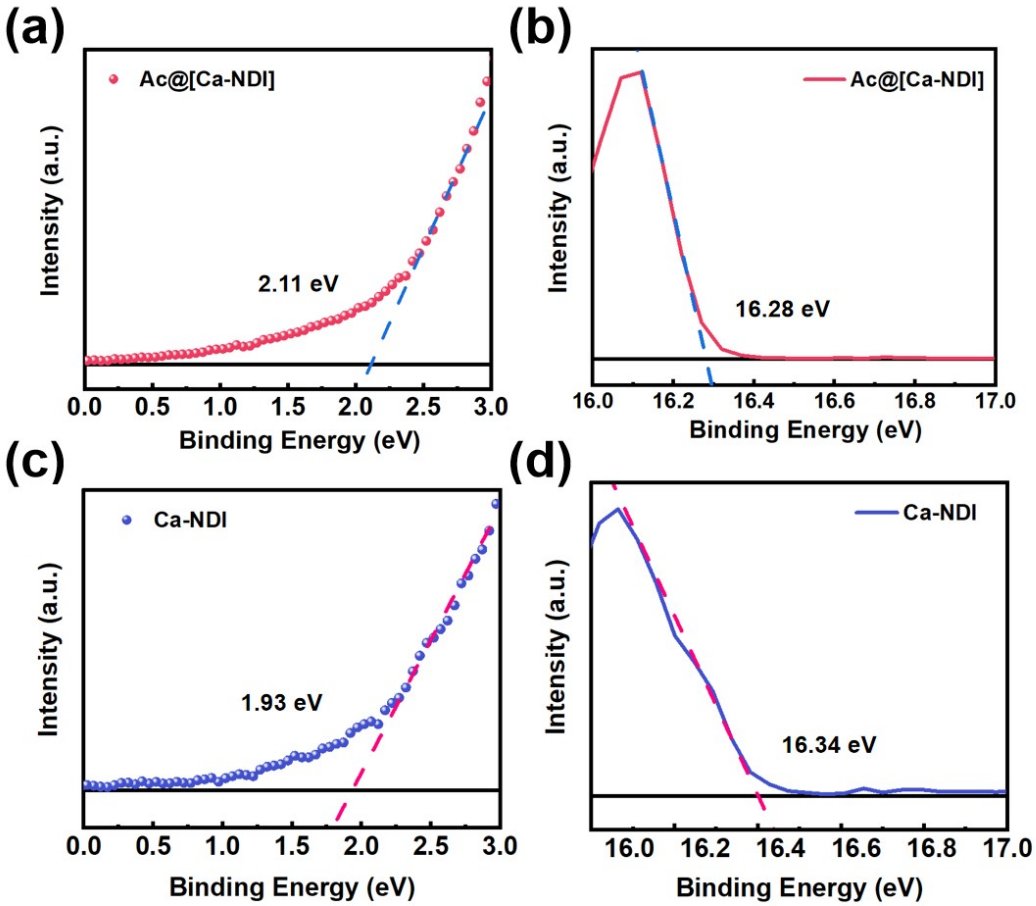

Figure S9. (a) and (c): Valence band edges of Ac@[Ca-NDI] MOCF and Ca-NDI MOF. (b) and (d): Secondary cutoff edges of Ac@[Ca-NDI] MOCF and Ca-NDI MOF.

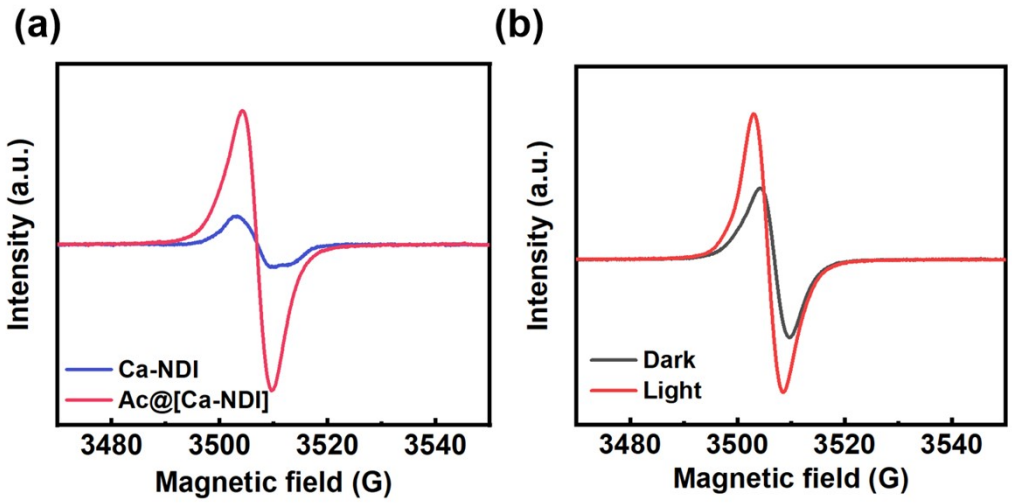

Figure S10. (a) ESR spectra of Ac@[Ca-NDI] MOCF and Ca-NDI MOF. (b) ESR spectra of Ac@[Ca-NDI] MOCF under dark and illuminated conditions.

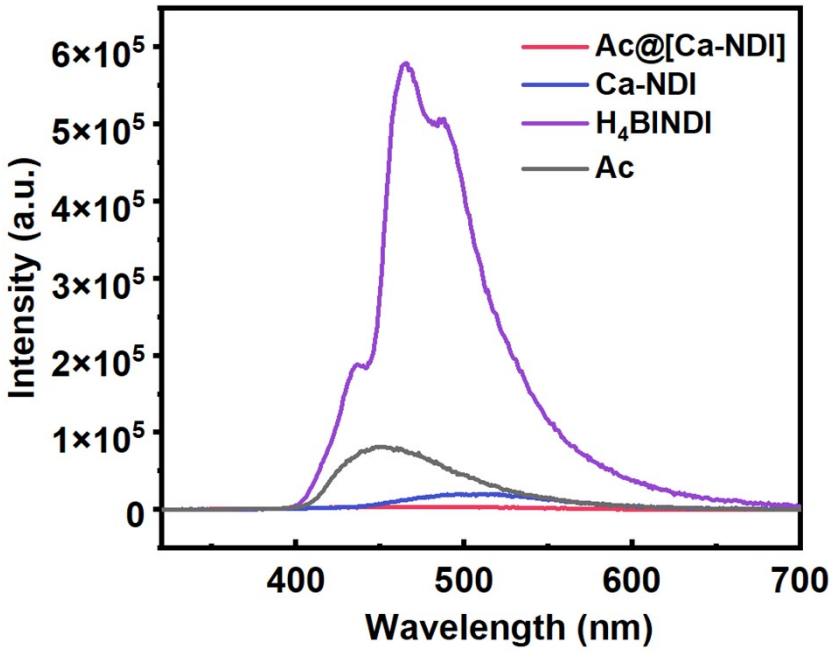

Figure S11. PL spectra.of Ac, H_4BINDI, Ca-NDI MOF and Ac@[Ca-NDI] MOCF.

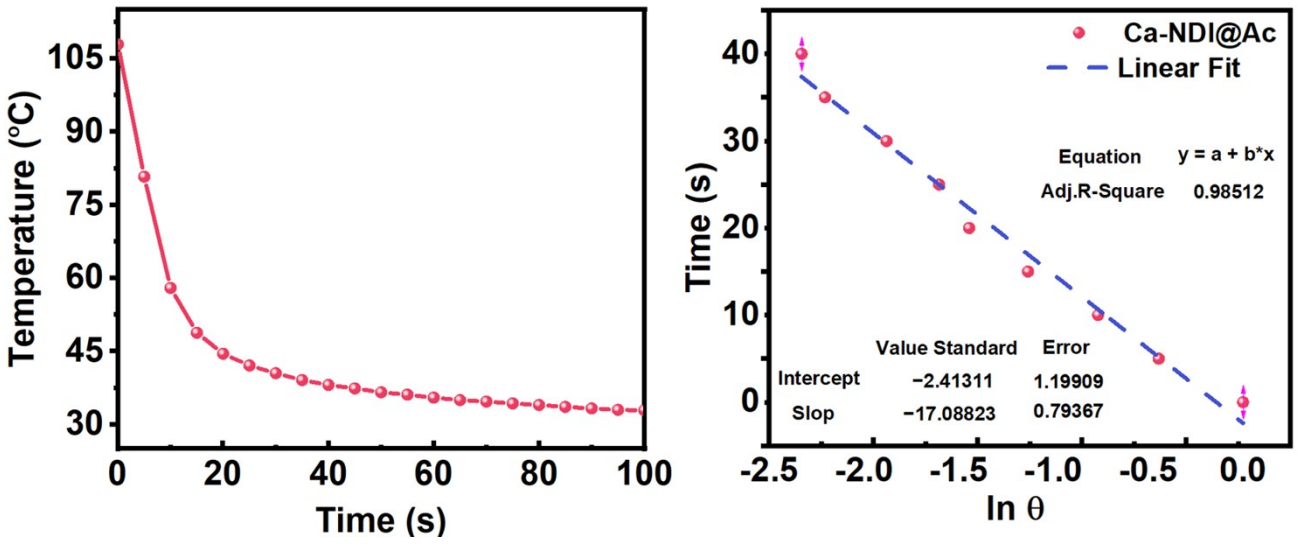

Figure S12. (a) Cooling curve and (b) corresponding linear fit of time (t) versus ln θ.

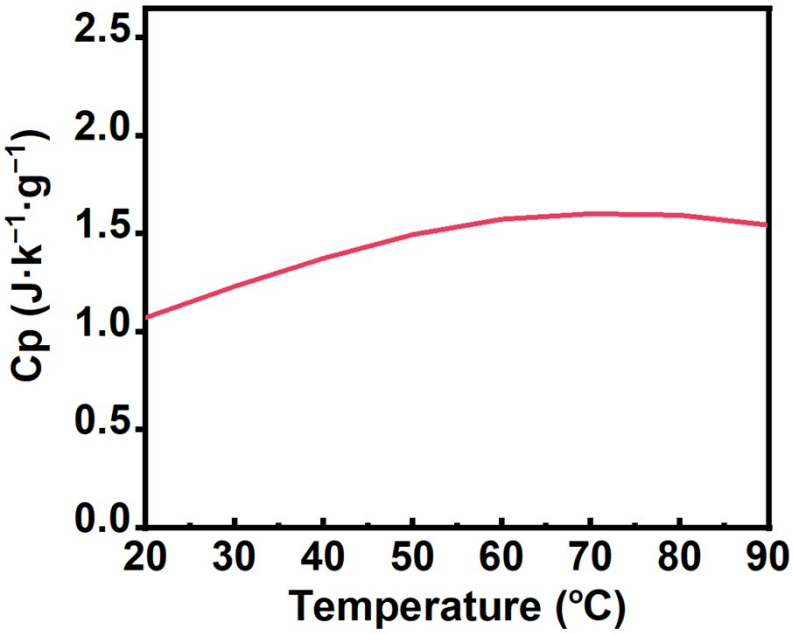

Figure S13. The DSC result of Ac@[Ca-NDI] MOCF.

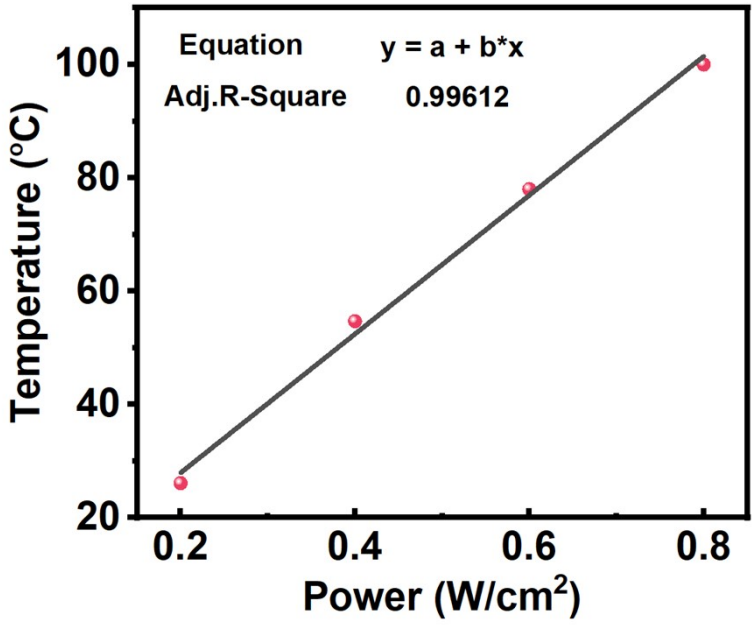

Figure S14. Linear fitting curve of temperature versus power density.

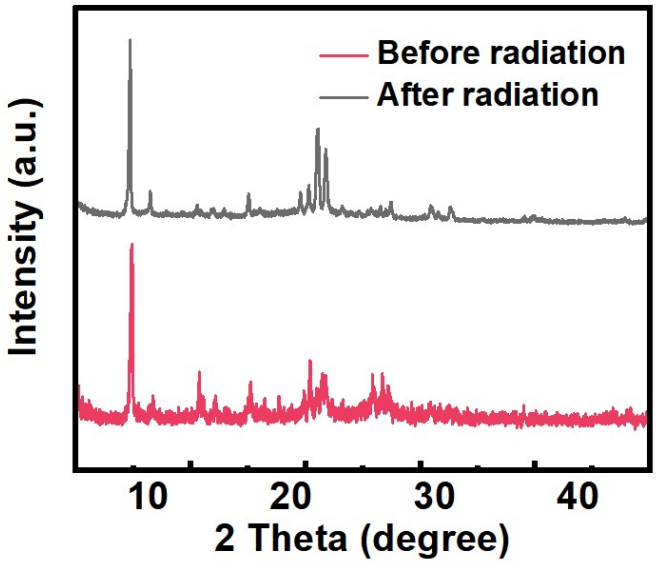

Figure S15. PXRD patterns of the Ac@[Ca-NDI] MOCF before and after irradiation.

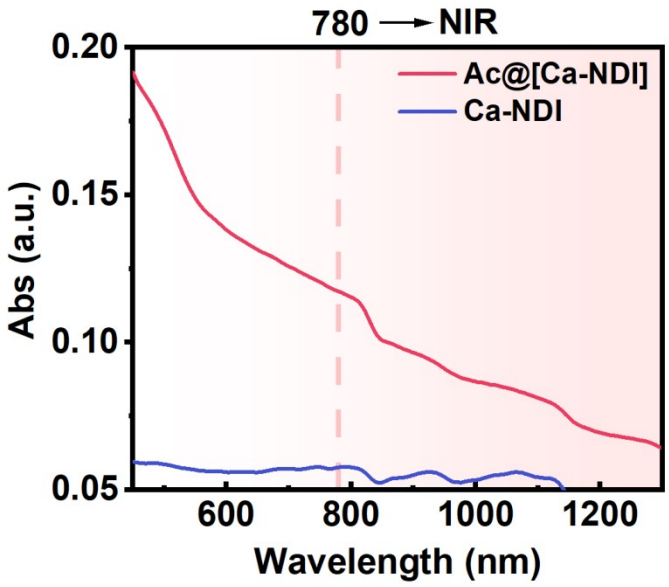

Figure S16. UV-Vis absorption spectra of Ac@[Ca-NDI] MOCF and Ca-NDI MOF in aqueous solution.

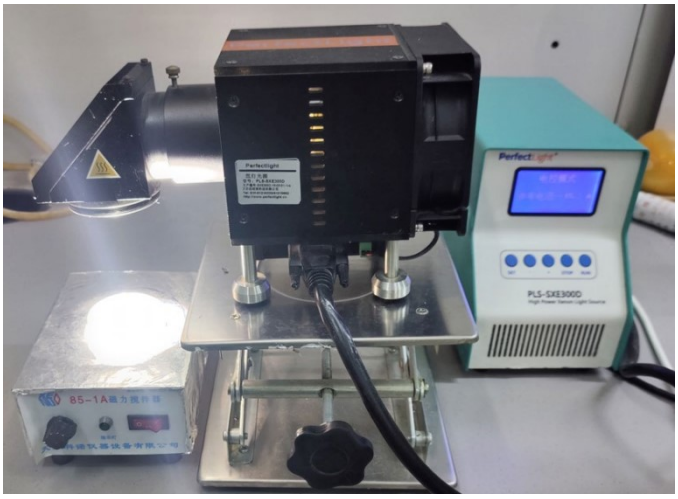

Figure S17. Schematic of the photothermal performance testing setup in Ac@[Ca-NDI] MOCF aqueous solution.

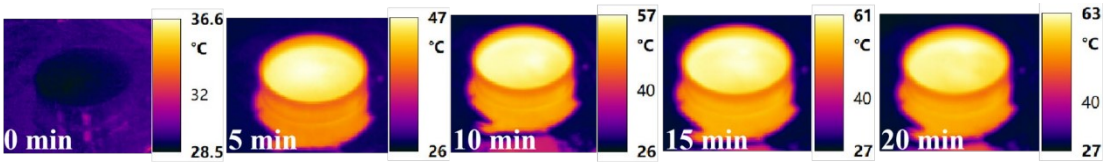

Figure S18. Infrared thermal imaging patterns of Ac@[Ca-NDI] MOCF aqueous solution.

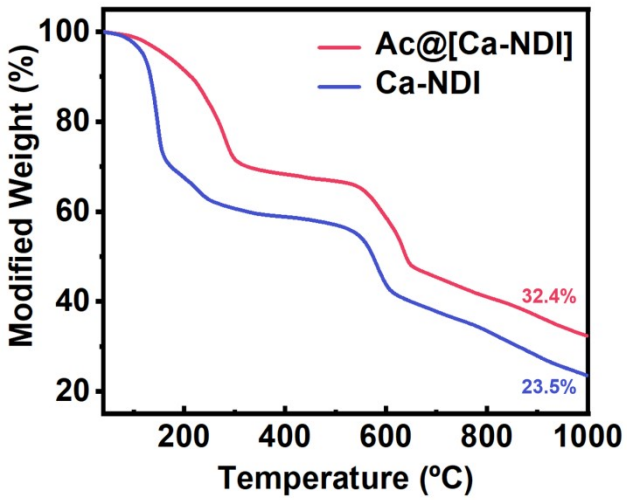

Figure S19. Thermogravimetric analysis spectra of Ac@[Ca-NDI] MOCF and Ca-NDI MOF.

Figure S20. The measurement results of the water contact angle of Ac@[Ca-NDI] MOCF.

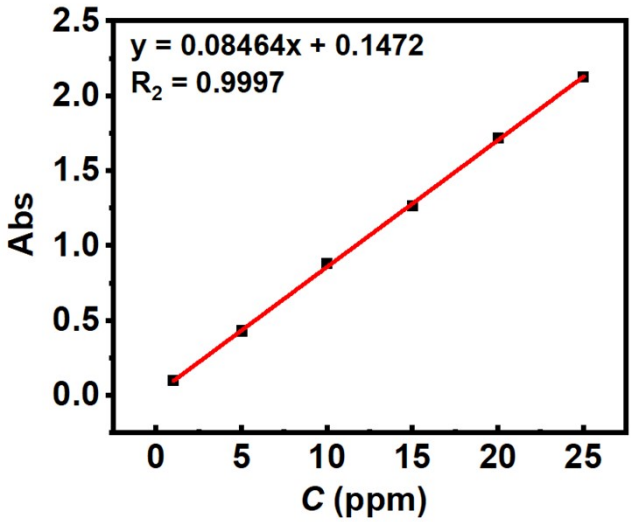

Figure S21. Calibration curve of phenol solution concentration.

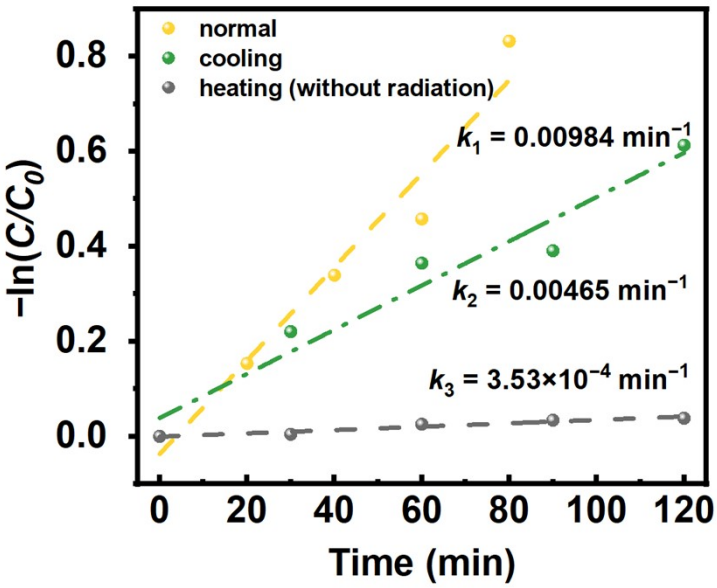

Figure S22. Catalytic rate curves for phenol degradation by Ac@[Ca-NDI] MOCF under different catalytic conditions with Xe lamp irradiation in the wavelength range of 300 nm < λ < 1200 nm.

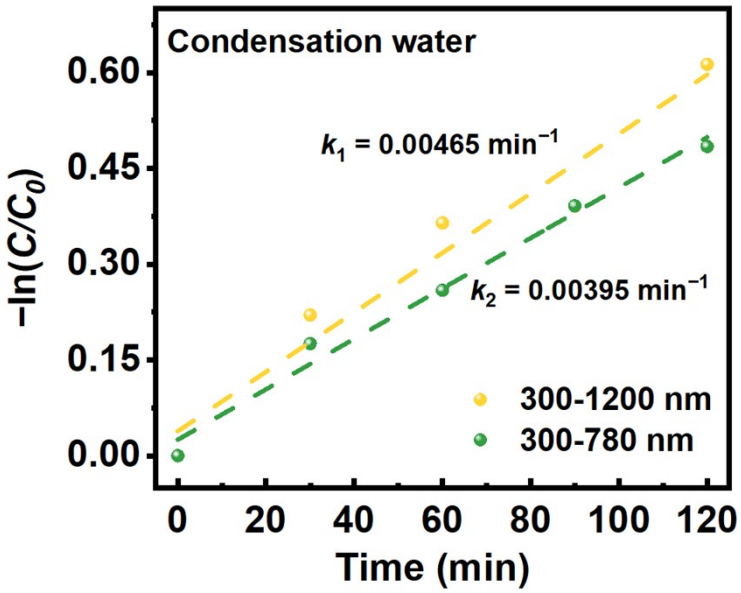

Figure S23. Catalytic rate curves for phenol degradation by Ac@[Ca-NDI] MOCF under Xe lamp irradiation at different wavelengths.

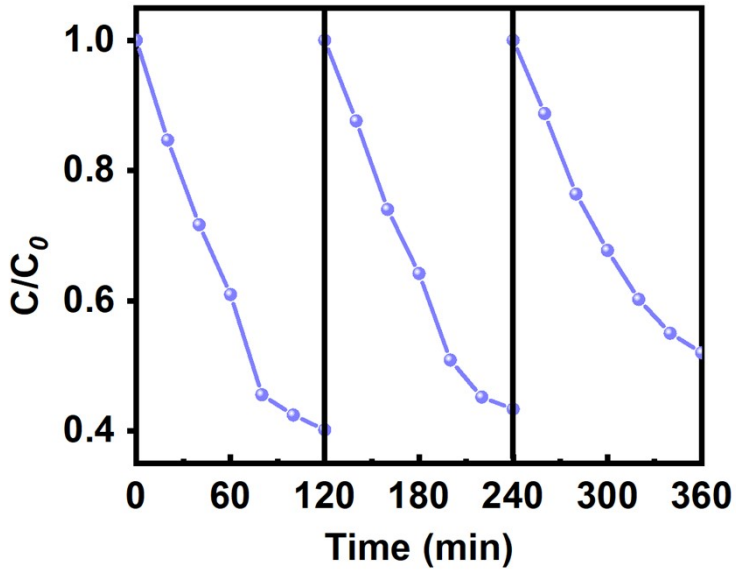

Figure S24. Phenol degradation cycling results of Ac@[Ca-NDI] MOCF.

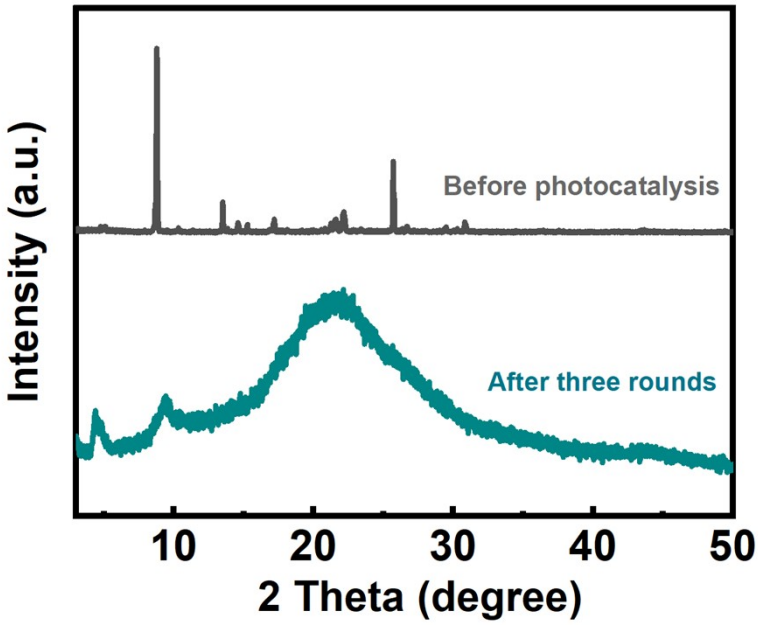

Figure S25. PXRD patterns of Ac @ [Ca NDI] MOCF before and after three cycles of photocatalysis.

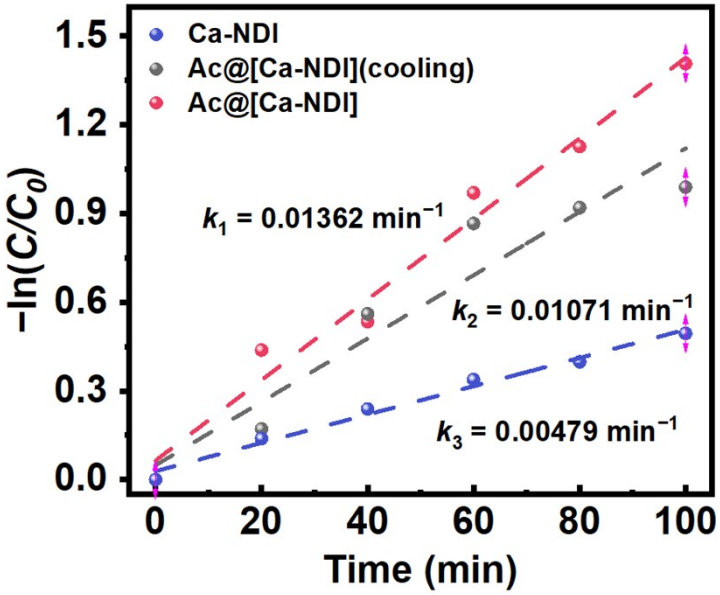

Figure S26. Catalytic rate curves for methyl orange degradation by Ac@[Ca-NDI] MOCF and Ca-NDI MOF.

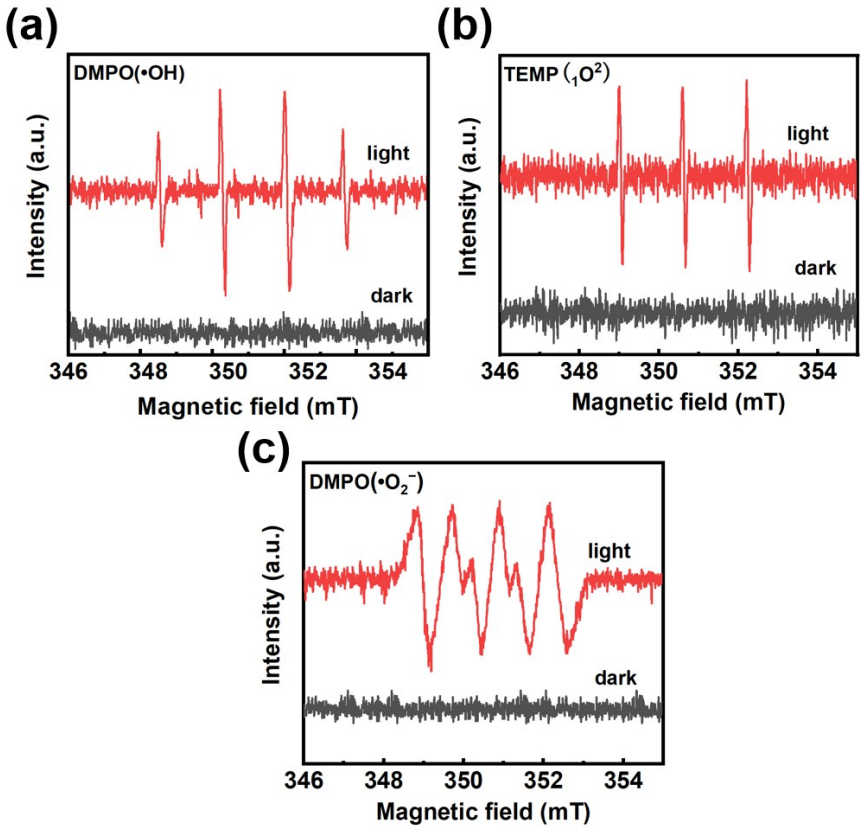

Figure S27. (a) EPR spectra of •OH (DMPO) under dark and illuminated conditions. (b) EPR spectra of

$^1O_2$ (TEMP) under dark and illuminated conditions. (c) EPR spectra of $\bullet O_2^-$ (DMPO) under dark and illuminated conditions.

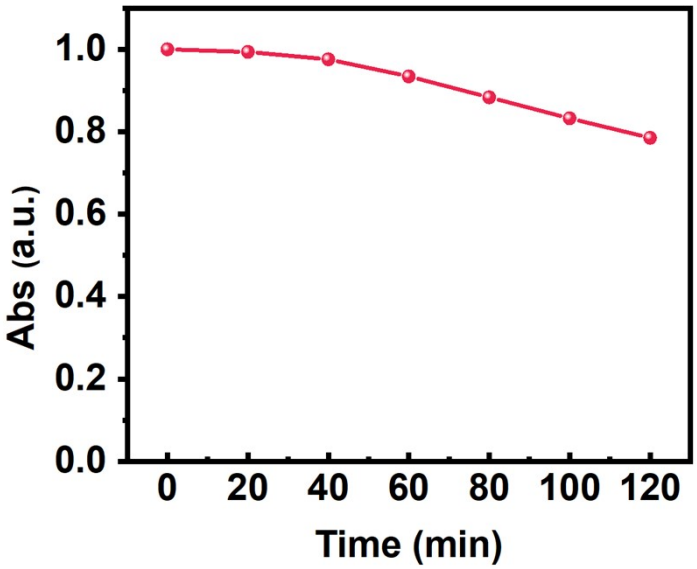

Figure S28. Degradation result of phenol by Ac@[Ca-NDI] MOCF under an argon atmosphere.

3. Supplementary Tables

Table S1. Crystal data of Ac@[Ca-NDI] MOCF.

CCDC Deposition Number	2457159
Empirical formula	$C_{76}H_{36}Ca_4N_6O_{25}$
Formula weight	1593.43
Temperature/K	100 K
Crystal system	monoclinic
Space group	*I*a
a/Å	24.8498(5)
b/Å	10.3567(2)
c/Å	33.9783(6)
α/°	90
β/°	90.339(2)
γ/°	90
Volume/Å^3	8744.6(3)
Z	4
ρ_{calc}g/cm^3	1.210
μ/mm^{-1}	2.776
F (000)	3256.0
Crystal size/mm^3	0.1 × 0.1 × 0.1
Radiation	Cu Kα (λ = 1.54184)

4. Supplementary Reference

[1] P. E. Blochl, Phys. Rev. B **1994**, *50*, 17953.

[2] J. Hafner, J. Comput. Chem. **2008**, *29*, 2044.

[3] V. Wang, N. Xu, J.-C. Liu, G. Tang, W.-T. Geng, Comput. Phys. Commun. **2021**, *267*, 108033.